remote sensing

MDPI

Article

MIMO: A Unified Spatio-Temporal Model for Multi-Scale Sea Surface Temperature Prediction

Siyun Hou [1,2], Wengen Li [1,*], Tianying Liu [1,2], Shuigeng Zhou [3,4], Jihong Guan [1], Rufu Qin [1,5] and Zhenfeng Wang [2]

[1] Department of Computer Science and Technology, Tongji University, Shanghai 200082, China; housiyun@tongji.edu.cn (S.H.); liutianying@tongji.edu.cn (T.L.); jhguan@tongji.edu.cn (J.G.); qinrufu@tongji.edu.cn (R.Q.)
[2] Project Management Office of China National Scientific Seafloor Observatory, Tongji University, Shanghai 200082, China; wangzhenfeng@cnsso.edu.cn
[3] Shanghai Key Lab of Intelligent Information Processing, Shanghai 200438, China; sgzhou@fudan.edu.cn
[4] School of Computer Science, Fudan University, Shanghai 200438, China
[5] State Key Laboratory of Marine Geology, Tongji University, Shanghai 200082, China
* Correspondence: lwengen@tongji.edu.cn

Abstract: Sea surface temperature (SST) is a crucial factor that affects global climate and marine activities. Predicting SST at different temporal scales benefits various applications, from short-term SST prediction for weather forecasting to long-term SST prediction for analyzing El Niño–Southern Oscillation (ENSO). However, existing approaches for SST prediction train separate models for different temporal scales, which is inefficient and cannot take advantage of the correlations among the temperatures of different scales to improve the prediction performance. In this work, we propose a unified spatio-temporal model termed the Multi-In and Multi-Out (MIMO) model to predict SST at different scales. MIMO is an encoder–decoder model, where the encoder learns spatio-temporal features from the SST data of multiple scales, and fuses the learned features with a Cross Scale Fusion (CSF) operation. The decoder utilizes the learned features from the encoder to adaptively predict the SST of different scales. To our best knowledge, this is the first work to predict SST at different temporal scales simultaneously with a single model. According to the experimental evaluation on the Optimum Interpolation SST (OISST) dataset, MIMO achieves the state-of-the-art prediction performance.

Keywords: sea surface temperature (SST); multi-scale SST prediction; spatio-temporal model; data fusion

Citation: Hou, S.; Li, W.; Liu, T.; Zhou, S.; Guan, J.; Qin, R.; Wan, Z. MIMO: A Unified Spatio-Temporal Model for Multi-Scale Sea Surface Temperature Prediction. *Remote Sens.* **2022**, *14*, 2371. https://doi.org/10.3390/rs14102371

Academic Editor: Yukiharu Hisaki

Received: 29 March 2022
Accepted: 12 May 2022
Published: 14 May 2022

1. Introduction

Sea surface temperature (SST) refers to the temperature of the water from 1 millimeter to 20 meters below the sea surface. The ocean covers about three-quarters of the Earth's surface and greatly influences global climate [1] and human activities [2]. As one key factor of ocean environment, SST affects global climate when assimilating and releasing heat. For instance, global precipitation is influenced by ocean evaporation, which is highly dependent on SST [3]. The widely known El Niño–Southern Oscillation (ENSO) phenomenon is an irregular periodic variation of SST in the tropical eastern Pacific Ocean, and occurs every 3∼5 years [4]. Therefore, accurately predicting SST could benefit various applications, e.g., weather forecasting, global warming prevention and extreme climate tracking.

Most existing methods for SST prediction are either numerical models or data-driven models. Numerical models [5], e.g., General Circulation Model (GCM), Integrated Forecast System (IFS) and Global Forecast Systems (GFS), predict SST by using differential equations to describe the relations between SST and other oceanic factors (e.g., sea surface height and air temperature) according to the laws of physics. Numerical models are usually of high complexity due to the large number of parameters, thus resulting in high computation cost. Data-driven SST prediction models predict SST by discovering the hidden regularity and

patterns in historical SST data, and can be further divided into three sub-categories, i.e., statistical models [6], shallow neural network models [7–9] and deep learning models [10–12]. In contrast to numerical models, data-driven models require less domain knowledge and usually can achieve better prediction performance.

The existing methods mentioned above all focus on single-scale SST prediction, e.g., predicting the SST of the next seven days, and predicting the monthly average SST in the next one year. However, single-scale SST prediction has some disadvantages. First, we have to train different models for predicting different scales of SST, which is inefficient and costs many computation resources. Second, single-scale SST prediction ignores the correlations among SST of different scales. In practice, SST has different scales of temporal regularity. For example, the short-term SST usually depends on the long-term trends and periodicity of SST. In this case, the correlations of different scales of SST could be used for improving SST prediction.

To overcome the disadvantages of existing SST prediction methods, we propose multi-scale SST prediction to predict daily, weekly and monthly SST simultaneously. To this end, we face some technical challenges. First, multi-scale SST prediction needs to learn the features that can capture the regularity of different temporal scales of SST. Second, it is nontrivial to exploit the correlations among SST data of different scales. Third, the prediction model should be able to adapt to different scales of SST prediction.

To address these challenges in multi-scale SST prediction, we propose a new spatio-temporal model, i.e., the Multi-In and Multi-Out (MIMO) model. Concretely, the MIMO model first learns the spatio-temporal features for different scales of SST with independent learning blocks. Then, the learned features are fused to obtain unified feature representation. Finally, the MIMO model adaptively predicts different scales of SST with different prediction components. This is the first work that achieves unified prediction for SST of different temporal scales. The proposed model can learn the spatio-temporal features of SST well and fully take advantage of the correlations among different scales of SST to enhance the prediction.

The main contributions of this work are highlighted as follows.

- We raise the multi-scale SST prediction problem and highlight its technical challenges.
- We propose the MIMO model that can predict SST at multiple scales simultaneously with a single model. MIMO learns different scales of temporal regularity in SST and can be adapted to the requirements of SST prediction at different scales.
- We conduct extensive experiments on real SST datasets to evaluate the proposed method, and the experimental results shows that MIMO outperforms existing SST prediction methods, including CNN, LeNet and ConvLSTM.

The remainder of this work is organized as follows. Section 2 reviews the related work on SST prediction and analyzes the disadvantages of existing methods. Section 3 formally defines the problem of multi-scale SST prediction, and Section 4 gives the technical details of the proposed MIMO model. Section 5 reports the experimental results. Finally, Section 6 concludes the work.

2. Background

As discussed previously, existing SST prediction methods can be classified into numerical models and data-driven models, where data-driven models can be further divided into statistical models, shallow neural network models and deep learning models. Figure 1 shows the taxonomy of existing SST prediction methods and their representative models.

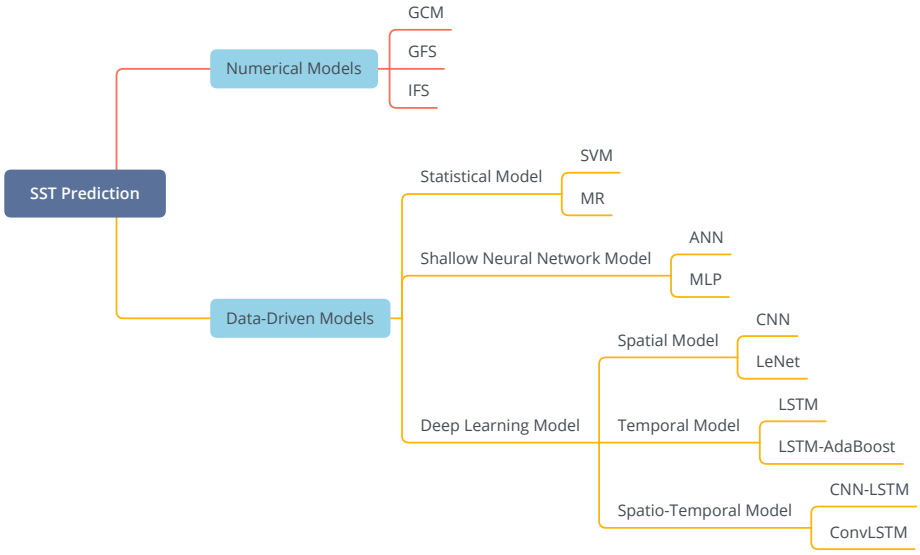

Figure 1. The taxonomy of existing SST prediction models.

2.1. Numerical Models

Numerical models utilize mathematical equations to describe the underlying regularity in SST and its correlations with other oceanic and atmospheric variables [13–15]. This requires a better understanding of the dynamics of SST to design the prediction models. Representative numerical SST prediction models include General Circulation Model (GCM), Integrated Forecast System (IFS) and Global Forecast Systems (GFS).

GCM simulates the changes of the global climate by calculating the hourly evolution of the atmosphere based on the conservation laws for atmospheric mass, momentum, total energy and water vapor [16]. For example, Krishnamurti et al. used 13 coupled atmosphere-ocean models to predict SST [17].

The IFS model and GFS model are developed by the European Centre for Medium-Range Weather Forecasts (ECMWF) and the Command National Centers for Environmental Prediction (NCEP), respectively [18]. The IFS model can predict the SST of the following 10–15 days while the GFS model can predict the SST of the following 16 days. Both models contain multiple GCMs and can also predict other variables of the ocean and atmosphere.

Numerical models are usually of high computational complexity due to the large number of mathematical equations they have. In addition, numerical models are widely used for analyzing the global trends of SST but cannot predict the SST of high spatial resolutions well.

2.2. Data-Driven Models

Different from numerical models, data-driven models directly learn knowledge from historical SST data with machine learning techniques to conduct the prediction. Therefore, data-driven models depend more on SST data than the domain knowledge in ocean climate and environment.

2.2.1. Statistical Models

Statistical models for SST prediction learn the regularity and hidden patterns of SST from historical data [19,20]. Representative statistical models include support vector machine (SVM) and multi-linear regression (MR) model. SVM constructs a set of hyperplanes in a high dimensional space and uses these hyperplanes for classification and regression. For example, Lins et al. developed an SVM model that uses historical daily SST as input to predict the SST across the Northeastern Brazilian Coast [21] and the tropical Atlantic [6]. The MR model combines the SST anomaly index with the tropical Pacific SST anomaly to predict SST. It takes 12 months of historical SST data as the input and assumes that the SST

follows some statistical assumptions. Then, the MR model uses a linearly weighted sum method to predict the SST of the following month [22]. Statistical models need feature engineering to extract features from SST data, which may result in the loss of some important information for SST prediction.

2.2.2. Shallow Neural Network Models

Shallow neural network (SNN) models are of high flexibility in fitting raw SST data [23–25]. Compared with the statistical models, SNN models can capture the nonlinear correlations in SST data, thus achieving better prediction performance. For instance, Patil et al. proposed an Artificial Neural Network (ANN) to predict the SST of the following 5 days [26]. Aparna et al. proposed an SNN that comprises three layers, i.e., input layer, linear layer and output layer, to predict the SST of the next day at specific locations [18]. Wei et al. separated SST time series data into monthly mean SST and monthly anomaly SST, and constructed two multilayer perceptron (MLP) models to generate the predicted results of SST [7].

Most shallow neural network models predict SST at some specific locations and ignore the spatial correlations and temporal regularity in SST. In addition, due to the limited learning ability, SNN models cannot fully exploit the large volume of historical SST data to train prediction models.

2.2.3. Deep Learning Models

With the substantial increase of SST data, statistical models and SNN models are unable to learn comprehensive knowledge from big SST data to further improve the prediction performance. Therefore, deep learning (DL) models have been introduced for SST prediction [27]. DL models can be classified into three sub-categories, i.e., deep spatial models, deep temporal models and deep spatio-temporal (ST) models.

Deep spatial models focus on learning the spatial correlations in SST data to achieve prediction. Ham et al. proposed a CNN-based model to predict the *Niño* 3.4 index of the next 12 months based on the historical SST data of 12 months [28]. Zheng et al. proposed a model with stacked multiple CNN layers, Max Pooling layers and upsampling layers to predict the SST of the next day using the historical SST data of 14 days [11].

Deep temporal models focus on learning the temporal regularity in SST data to achieve prediction. Zhang et al. proposed an LSTM model to predict the SST in the next three days in the East China Sea with the historical SST data of 15 days [10]. Xiao et al. combined Ada-Boost and LSTM to predict the SST in the next 10 days in the East China Sea with the historical SST data of 40 days [29]. Yao et al. proposed an encoder–decoder model based on LSTM to predict the SST in the next 10 days using the historical data of 10 days [30].

Deep spatio-temporal models learn both spatial correlations and temporal regularity in SST to achieve prediction. Xiao et al. proposed a multi-layer convolutional LSTM model to predict the SST in the next 10 days with the historical SST data of 50 days in the East China Sea [12]. Weyn et al. combined the ConvLSTM model and the CNN model to predict the SST of the next three days with the historical SST data of 12 days [31]. Zhang et al. proposed a CNN-LSTM-based model to predict the SST in the next eight months using the historical SST data of 28 months [32]. In addition, deep graph models have also been used for SST prediction in recent years. Zhang et al. proposed a graph model MGCN that uses historical SST data of six days to predict the SST of the next three days. They used a temporal convolution to learn the temporal features of SST which are then put into the graph model to learn the spatial features [33].

In general, deep learning models can achieve better prediction performance than statistical models and shallow neural network models. However, all existing data-driven models only consider single-scale SST prediction, i.e., predicting daily or monthly SST separately, and cannot achieve multi-scale SST prediction.

3. Problem Definition

For SST prediction, we usually divide the target region of interest R into small grid regions of the same size along the latitude and longitude, and then predict the SST for each grid region. For example, as illustrated in Figure 2, the region *Niño* 3.4 can be divided into 40×200 grid regions of size $0.25^\circ \times 0.25^\circ$.

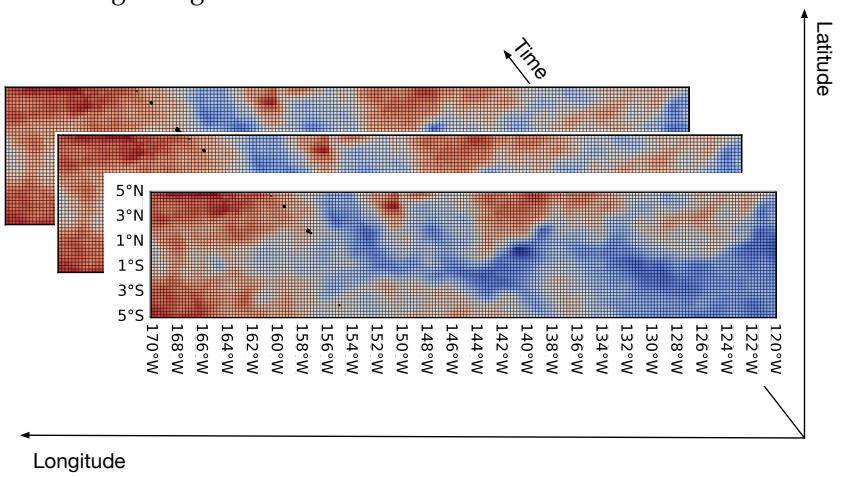

Figure 2. The daily SST sequence for the region of *Niño* 3.4, which is located within [5°N∼5°S, 120°W∼170°W] in the Pacific Ocean and divided into 40×200 grid regions of size $0.25^\circ \times 0.25^\circ$.

Assuming that the region of interest R is divided into $c \times d$ grid regions, the corresponding SST records at time slot t are denoted by $X_t \in \mathbb{R}^{c \times d}$. Data-driven SST prediction methods learn the underlying patterns of SST from historical SST data to predict the SST in the future. Specifically, the problem of single-scale SST prediction is defined as below.

Definition 1 (**Single-Scale SST Prediction**). *Given a sequence of historical SST records* $\mathbf{X}_{t-a+1\to t} = (\mathbf{X}_{t-a+1}, \mathbf{X}_{t-a+2}, \ldots, \mathbf{X}_t)$ *of length a, single-scale SST prediction aims to predict the SST sequence* $\mathbf{X}_{t+1\to t+b} = (\mathbf{X}_{t+1}, \mathbf{X}_{t+2}, \ldots, \mathbf{X}_{t+b})$ *of length b in the future, i.e.,*

$$\mathbf{X}_{t+1\to t+b} = \arg\max_{\mathbf{X}_{t+1\to t+b}} p(\mathbf{X}_{t+1\to t+b} | \mathbf{X}_{t-a+1\to t}) \tag{1}$$

In general, the time slot in single-scale SST prediction could be daily, weekly and monthly. For example, we can have the following SST prediction schemes:

- Using the historical daily SST of 10 days to predict the daily SST of the following seven days, where $a = 10$ and $b = 7$;
- Using the historical monthly SST of 36 months to predict the monthly SST of the following 12 months, where $a = 36$ and $b = 12$.

In existing studies on SST prediction, different scales of SST prediction are treated separately, i.e., training different prediction models for different scales of SST prediction. In this work, we aim to unify the prediction for multiple scales of SST and propose the problem of multi-scale SST prediction as defined below.

Definition 2 (**Multi-scale SST prediction**). *Given daily, weekly and monthly historical SST records* $\mathbf{X}^{daily}_{t-a+1\to t}$, $\mathbf{X}^{weekly}_{t-a+1\to t}$ *and* $\mathbf{X}^{monthly}_{t-a+1\to t}$, *respectively, multi-scale SST prediction aims to predict their corresponding records in the next b time slots, i.e.,*

$$\left\{\mathbf{X}^{daily}_{t+1\to t+b}, \mathbf{X}^{weekly}_{t+1\to t+b}, \mathbf{X}^{monthly}_{t+1\to t+b}\right\} = \arg\max_{\left\{\mathbf{X}^{daily}_{t+1\to t+b}, \mathbf{X}^{weekly}_{t+1\to t+b}, \mathbf{X}^{monthly}_{t+1\to t+b}\right\}} \tag{2}$$

$$p\left(\left\{\mathbf{X}^{daily}_{t+1\to t+b}, \mathbf{X}^{weekly}_{t+1\to t+b}, \mathbf{X}^{monthly}_{t+1\to t+b}\right\} \middle| \left\{\mathbf{X}^{daily}_{t-a+1\to t}, \mathbf{X}^{weekly}_{t-a+1\to t}, \mathbf{X}^{monthly}_{t-a+1\to t}\right\}\right)$$

Figures 3 and 4 illustrate the difference between single-scale SST prediction and multi-scale SST prediction. Single-scale SST prediction uses the same scale of historical SST data to predict the corresponding future SST records. Therefore, in single-scale SST prediction, the input has three dimensions, i.e., latitude, longitude and time slots. In contrast, multi-scale SST prediction considers multiple scales of historical SST data and achieves the prediction for all the scales of SST together, thus covering short-term, mid-term and long-term SST prediction. Therefore, in multi-scale SST prediction, the input has four dimensions, i.e., latitude, longitude, time slots and scales.

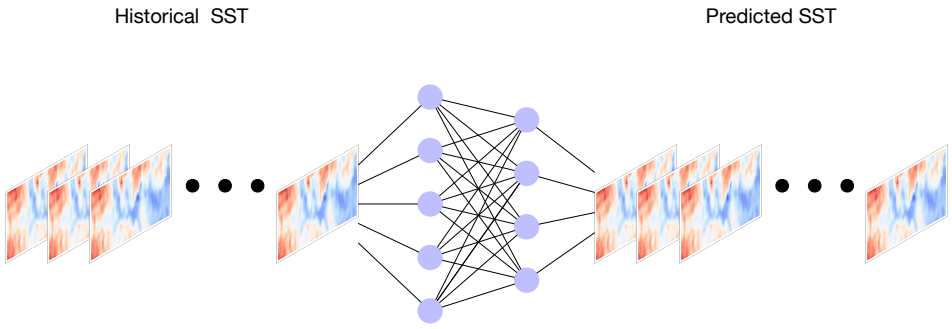

Figure 3. Single-scale SST prediction that uses the historical SST of single scale to predict the future single-scale SST.

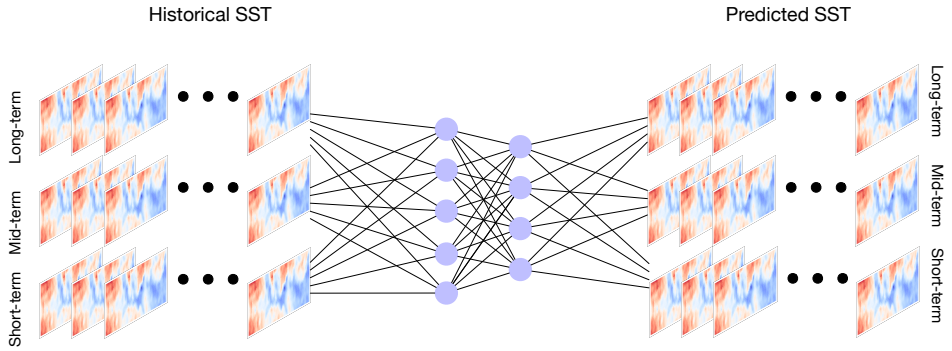

Figure 4. Multi-scale SST prediction that uses different scales, e.g., daily, weekly and monthly, of historical SST data to predict their future records simultaneously.

Considering that the prediction periods of most existing SST prediction methods are less than 12 time slots, we use the daily, weekly and monthly SST records of 36 time slots to predict the daily, weekly and monthly SST records in the next 12 time slots, i.e., $a = 36$ and $b = 12$. With such a setting, we can cover most of the prediction schemes in existing studies.

4. Methodology

Figure 5 presents the overall architecture of the MIMO model which consists of an input layer, an encoder and a decoder. The input layer contains multi-scale SST data and some external factors, where external factors, including short wave radiation (SWR) and long wave radiation (LWR), are regarded as important influence factors for SST and are thus introduced to enrich the information for SST prediction. Considering that the spatial resolutions of SST data and external factors are usually different due to the difference in the ways of data collection, we use Bicubic Convolutional Interpolation (BCI) to align the spatial resolutions of external factors to that of SST data. The technical details of BCI are discussed in Appendix A.

In the encoder, MIMO uses five independent Zoom In Spatio-Temporal (ZIST) blocks to learn the hierarchical spatio-temporal features from multi-scale SST data and external factors and uses Cross Scale Fusion (CSF) to fuse the learned features. In the decoder, MIMO

designs three independent components for monthly, weekly and daily SST prediction, respectively. Each component comprises three Zoom Out Spatio-Temporal (ZOST) blocks and one Full Connection (FC) layer, where ZOST blocks decode the fused features from the encoder stage and the FC layer achieves the final prediction.

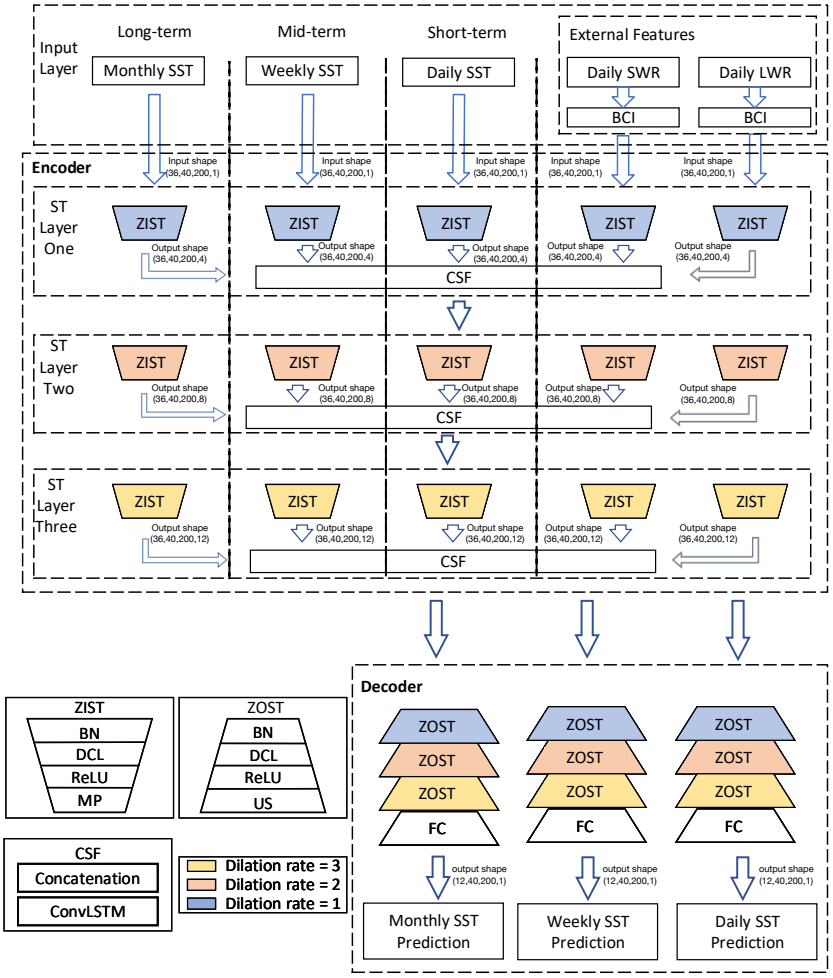

Figure 5. The architecture of MIMO model which consists of an input layer, an encoder and a decoder. The input layer contains multi-scale SST data and some external factors. The encoder contains three spatio-temporal layers and each layer contains five independent Zoom In Spatio-Temporal (ZIST) blocks, where each ZIST block consists of Batch Normalization (BN), Dilated ConvLSTM (DCL), Rectified Linear Unit (ReLU) and Max Pooling (MP). The decoder contains three components for monthly, weekly and daily SST prediction, respectively, and each component contains three Zoom Out Spatio-Temporal (ZOST) blocks and one Full Connection (FC) layer, where each ZOST block consists of BN, DCL, ReLU and Up Sampling (US).

4.1. Encoder

The encoder of the MIMO model has three spatio-temporal (ST) layers, and each ST layer consists of five Zoom In Spatio-Temporal (ZIST) blocks and one Cross Scale Fusion (CSF) sub-layer.

4.1.1. Zoom in Spatio-Temporal Block

Each ZIST block comprises Batch Normalization (BN), Dilated ConvLSTM (DCL), Rectified Linear Unit (ReLU) and Max Pooling (MP), where BN normalizes the data to avoid overfitting, DCL learns hierarchical features from the data using dilated convolution, ReLU filters the negative values to speed up the training process and MP reduces the number of model parameters and alleviates the position sensitivity.

Specifically, the DCL uses the dilated convolutional operation to replace the Hadamard product in LSTM to capture more spatial features. Figure 6 illustrates the 2D dilated convolutional operations that use intermittent connections between grids in traditional convolutional kernels. The dilation rate r is used to quantify the distance of intermittent connections between grids. Given a $k \times k$ convolutional kernel, the corresponding dilated kernel size is $k_d = k + (k-1)(r-1)$. For example, in Figure 6, $r = 1$ corresponds to a normal convolution kernel, $r = 2$ corresponds to a dilated convolution kernel of size $k_d = 5$, and $r = 3$ corresponds to a dilated convolution kernel of size $k_d = 7$.

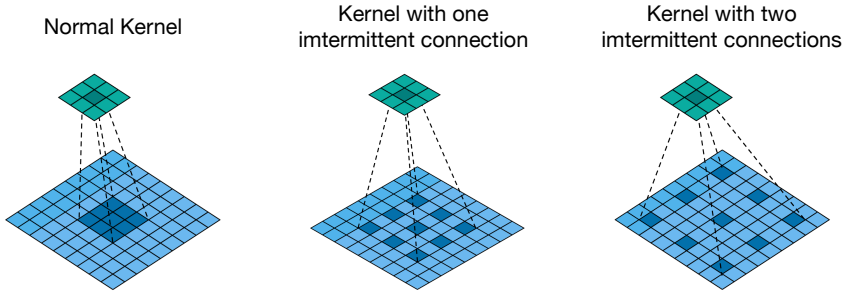

Figure 6. The normal convolutional kernel and dilation convolutional kernels.

DCL will face the "gridding" issue [34] when multiple ST layers are stacked. To address this issue, MIMO sets different dilation rates r, i.e., 1, 2 and 3, for three ST layers, respectively.

In addition, the features learned by DCL can be affected by the changes of position, which makes the prediction model sensitive to specific positions and shapes. Meanwhile, with multiple stacked DCLs, we may lose the features for the marginal areas of feature maps. Both issues will damage the generalization of the MIMO model. We introduce Max Pooling (MP) to address these two issues. MP can reduce the model size and indirectly increase the receptive field of the kernel size to better learn spatial features in the data. In addition, MP brings the advantage of feature invariance to the prediction model, which avoids the learning errors due to location changes.

4.1.2. Cross Scale Fusion

MIMO learns the spatio-temporal features of different scales of SST and external features separately, and then fuses them together. Concretely, in each ST layer, the features learned from five ZISTs are fused with the CSF sub-layer. Each CSF sub-layer is a ConvLSTM layer with kernel size of 1×1. As illustrated in Figure 7, CSF can reduce the dimensions of the outputs from five ZISTs to achieve the fusion.

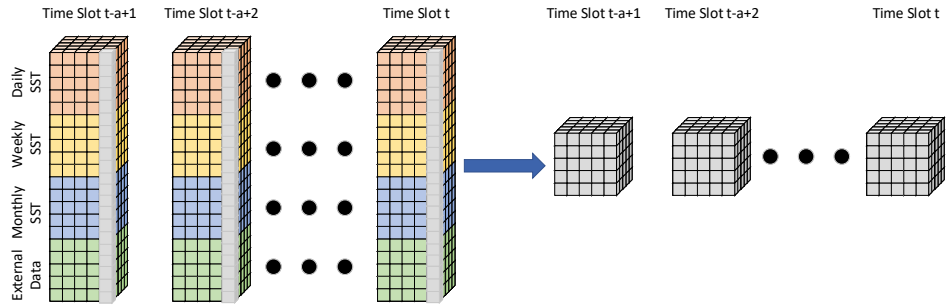

Figure 7. The structure of the Cross Scale Fusion (CSF) sub-layer, where the learned spatio-temporal features of different scales of SST and external features.

4.2. Decoder

The decoder of the MIMO model comprises three independent components, each consisting of three Zoom Out Spatio-Temporal (ZOST) blocks and one Full Connection (FC)

layer. As illustrated in Figure 5, each ZOST comprises BN, DCL, ReLU and Up Sampling (US) and can decode the fused features from the encoder to the target scale of SST.

We use the nearest neighbor upsampling method to decode the features from the encoder. The nearest upsampling method directly enlarges the fused features in proportion to the input data. As illustrated in Figure 8, the 2×2 feature map is converted to a 4×4 feature map using upsampling with 2×2 filters.

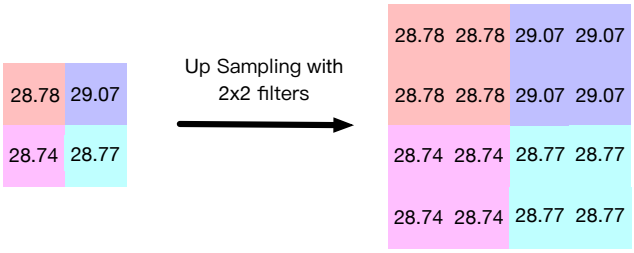

Figure 8. The upsampling that recovers the shape of the input data.

4.3. Loss Function

The objective of the MIMO model is to minimize the total error of the SST predictions of multiple scales, i.e.,

$$Loss = \sum_{i=1}^{3} \alpha_i L_i(\mathbf{X}_i^{obs}, \hat{\mathbf{X}}_i^{pre}) \tag{3}$$

where L_i is the loss function for the i-th scale of SST, α_i is the weight parameter for loss function L_i, $\mathbf{X}_i^{obs}$ is the ground truth and $\hat{\mathbf{X}}_i^{pre}$ is the predicted result of the MIMO model.

Since different scales of SST have different effects on the MIMO model, the loss functions corresponding to different scales of SST also have different effects on the total loss function. If we calculate the loss functions for SST predictions of different scales separately, the convergence speed of each loss function will be inconsistent. Hence, the MIMO model introduces weight parameters, i.e., α_i, to balance the convergence speed between the loss functions for different scales of SST prediction. According to the experimental analysis, we set the weights for the loss functions of daily, weekly and monthly scales of SST prediction to 0.6, 0.2 and 0.2, respectively.

The loss function L_i for the i-th scale of SST is the mean squared error (MSE), calculated as below.

$$L_i = \frac{1}{n} \sum (X^{obs} - \hat{X}^{pre})^2 \tag{4}$$

where n is the number of samples. During the training, the model is optimized using Nadam [35].

5. Model Evaluation

We used the SST data from the El Niño region to compare the accuracy of our model to SVM, CNN, LeNet, LSTM and ConvLSTM. The time range of the SST dataset is from 1 January 1982 to 31 December 2019.

5.1. Datasets

We use the Optimum Interpolation SST (OI-SST) data from the National Oceanic and Atmospheric Administration (NOAA) and select the region of *Niño* 3.4 as the target region for prediction. The NOAA 0.25° OI-SST is a long-term climate data record that incorporates the observations from different platforms, e.g., satellites, ships, buoys and Argo floats, into a regular global grid format. The *Niño* 3.4 region covers the area of [5°00′N∼5°00′S, 120°00′W∼170°00′W] and is divided into 40×200 grids of size $0.25° \times 0.25°$. In addition, the data for the external factors SWR and LWR are from NCEP/NCAR Reanalysis 1.

The whole dataset is divided into three subsets for training, validation and testing, respectively. The ratio of the three subsets is 72:1. Concretely, the training dataset contains 8956 samples, the validation dataset has 2239 samples and the testing dataset has 1244 samples. In the experiments, we aim to predict the daily, weekly and monthly SST records in the next 12 time slots. The number of iterations for model training is set to 1000 and the training process could end early if the loss function no longer changes for 10 consecutive rounds. The experiments run on a 64-core Intel Xeon processor with 256 GB RAM and 3 NVIDIA RTX 2080Ti GPUs. All SST prediction models are implemented based on TensorFlow 1.15.0.

5.2. Evaluation Metrics

We use four evaluation metrics to measure the performance of SST prediction models. The equations of the four evaluation metrics are listed as follows.

$$\text{MSE} = \frac{1}{n}\sum_i (x_i - \hat{x}_i)^2, \tag{5}$$

$$\text{RMSE} = \sqrt{\frac{1}{n}\sum_i (x_i - \hat{x}_i)^2}, \tag{6}$$

$$\text{MAE} = \frac{1}{n}\sum_i |x_i - \hat{x}_i|, \tag{7}$$

$$\text{MAPE} = \frac{100\%}{n}\sum_i \left|\frac{x_i - \hat{x}_i}{x_i}\right|. \tag{8}$$

where $\hat{x}$ and x are the predicted value and the observed value, respectively, and n is the total number of predicted samples.

5.3. Results

5.3.1. Weight Evaluation

To decide the values for the weights α_i $(i = 1, 2, 3)$ in the loss function, we evaluate the performance of MIMO models with different settings as below, where L_1, L_2 and L_3 correspond to the loss functions of daily, weekly and monthly predictions, respectively.

- **MIMO-122**: $L_1 = 1$, $L_2 = 2$ and $L_3 = 3$.
- **MIMO-911**: $L_1 = 0.9$, $L_2 = 0.1$ and $L_3 = 0.1$.
- **MIMO**: $L_1 = 0.6$, $L_2 = 0.2$ and $L_3 = 0.2$.
- **MIMO-433**: $L_1 = 0.4$, $L_2 = 0.3$ and $L_3 = 0.3$.
- **MIMO-244**: $L_1 = 0.2$, $L_2 = 0.4$ and $L_3 = 0.4$.

Table 1 presents the results of these models, where the best results are highlighted by boldface. As suggested by the table, MIMO-911 and MIMO achieve comparable performance and outperform all the other prediction models. Considering that MIMO has the best performance in predicting weekly and monthly SST and also achieves a high accuracy in predicting daily SST, we thus set $L_1 = 0.6$, $L_2 = 0.2$ and $L_3 = 0.2$ in the following experiments.

Table 1. The results of MIMO with different settings for the weights of loss function.

Model	Daily				Weekly				Monthly				Total MSE
	MSE	RMSE	MAE	MAPE	MSE	RMSE	MAE	MAPE	MSE	RMSE	MAE	MAPE	
MIMO-122	2.08	1.44	1.18	4.31%	1.88	1.37	1.11	4.07%	1.37	1.17	0.96	3.55%	1.99
MIMO-911	**0.37**	**0.61**	**0.47**	**1.76%**	0.61	0.78	0.60	2.22%	0.81	0.90	0.72	2.63%	**0.44**
MIMO	0.40	0.63	0.49	1.81%	**0.50**	**0.71**	**0.55**	**2.04%**	**0.58**	**0.76**	**0.60**	**2.24%**	0.45
MIMO-433	0.46	0.68	0.53	1.95%	0.58	0.76	0.60	2.20%	0.66	0.82	0.64	2.37%	0.56
MIMO-244	2.14	1.46	1.19	4.34%	2.01	1.42	1.14	4.19%	1.41	1.19	0.97	3.59%	1.80

5.3.2. Model Comparison

To verify the effectiveness of the MIMO model, we compare it with five representative forecasting models: CNN, ConvLSTM, LeNet, LSTM and SVM. The experimental results are shown in Table 2, where the best results are highlighted by boldface. The MIMO model has the best total MSE. LeNet and SVM also achieve good prediction performance and largely outperform CNN, ConvLSTM and LSTM. Concretely, the MIMO model has the best performance in predicting weekly and monthly SST. MIMO also achieves comparable performance with LeNet in predicting daily SST on MAE and MAPE. The MIMO model is designed for multi-scale SST prediction and needs to balance the prediction performance of different scales. Therefore, the MIMO model can achieve accurate predictions for all three scales of SST.

Table 2. The results of different SST prediction models.

Model	Daily				Weekly				Monthly				Total MSE
	MSE	RMSE	MAE	MAPE	MSE	RMSE	MAE	MAPE	MSE	RMSE	MAE	MAPE	
MIMO	**0.40**	**0.63**	0.49	1.81%	**0.50**	**0.71**	**0.55**	**2.04%**	**0.58**	**0.76**	**0.60**	**2.24%**	**0.45**
ConvLSTM	2.78	1.67	1.36	5.01%	2.86	1.69	1.40	5.11%	2.53	1.59	1.33	4.80%	2.75
LeNet	0.41	0.64	**0.47**	**1.77%**	0.99	0.99	0.76	2.86%	1.52	1.23	0.95	3.59%	0.58
CNN	1.20	1.10	0.84	3.09%	1.73	1.32	1.05	3.88%	2.82	1.68	1.35	5.09%	1.42
LSTM	2.04	1.41	1.15	4.24%	1.88	1.35	1.10	4.01%	1.39	1.16	0.95	3.53%	1.88
SVM	0.43	0.64	0.48	**1.77%**	0.82	0.90	0.71	2.62%	1.13	0.96	0.85	3.18%	0.61
LeNet with EXT	0.56	0.75	0.56	2.09%	1.62	1.27	1.00	3.69%	1.54	1.24	0.99	3.75%	0.97
LSTM with EXT	1.86	1.34	1.10	4.04%	1.80	1.32	1.08	3.98%	1.36	1.15	0.94	3.49%	1.75
SVM with EXT	1.33	1.14	0.91	3.35%	1.21	1.09	0.86	3.13%	1.04	1.01	0.82	3.00%	1.25

In addition, we add more experiments to evaluate the influence of external factors, i.e., short wave radiation (SWR) and long wave radiation (LWR). In accordance with Table 2, after including the external factors, the performance of LSTM has a small increase while the performance of LeNet and SVM decreases. This is because some models cannot handle external factors well and the contribution of these external factors is also limited. In addition, our MIMO model still outperforms these models with external factors, which indicates that the MIMO model can fully take advantage of the correlations among SSTs of different scales to improve the prediction.

5.3.3. Visualization

To better demonstrate the effectiveness of the MIMO model, we visualize the mean absolute errors of MIMO, ConvLSTM, LeNet and CNN for daily, weekly and monthly SST prediction in Figures 9–11, respectively.

As shown in Figure 9, MIMO and LeNet have similar MAE in daily SST prediction. The MAE of these two models is less than 0.5 for most grid regions. In contrast, the MAE of ConvLSTM is quite large. As for CNN, the predicted results for the 4th, 8th and 11th days are also bad.

Figure 10 illustrates the MAE for weekly SST prediction. MIMO has the best prediction performance among four models and its MAE errors are less than 0.5 for most grid regions. With the increase of time, the MAE of LeNet becomes large and reaches 1.25 for some grid regions. The MAEs of ConvLSTM and CNN are still very large but CNN performs better than ConvLSTM.

Figure 11 illustrates the MAE for monthly SST prediction. MIMO also achieves the best prediction performance. For LeNet, the MAE becomes larger than that of weekly SST prediction and still outperforms ConvLSTM and CNN. The MAE errors of ConvLSTM and CNN even reach 2.0 for some grid regions.

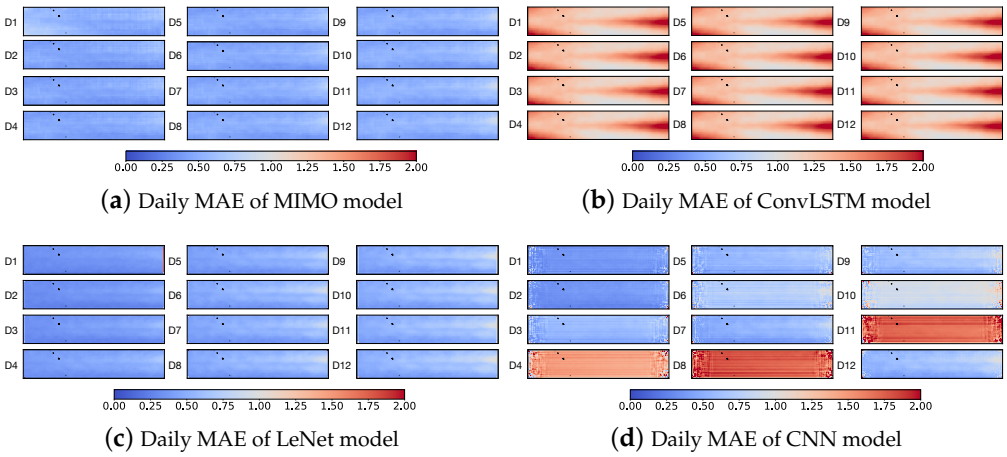

(**a**) Daily MAE of MIMO model (**b**) Daily MAE of ConvLSTM model

(**c**) Daily MAE of LeNet model (**d**) Daily MAE of CNN model

Figure 9. The results of daily SST prediction in *Niño* 3.4 region.

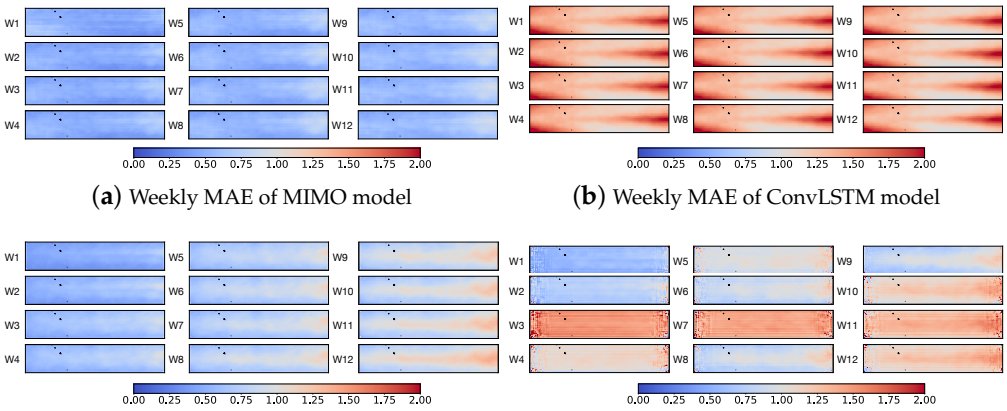

(**a**) Weekly MAE of MIMO model (**b**) Weekly MAE of ConvLSTM model

(**c**) Weekly MAE of LeNet model (**d**) Weekly MAE of CNN model

Figure 10. The results of weekly SST prediction in *Niño* 3.4 region.

In sum, in accordance with Figures 9–11, the MIMO model can achieve quite good prediction performance in all daily, weekly and monthly SST prediction. LeNet also achieves good prediction performance on daily SST prediction but has larger prediction errors than MIMO in weekly and monthly SST prediction. Both MIMO and LeNet largely outperform ConvLSTM and CNN.

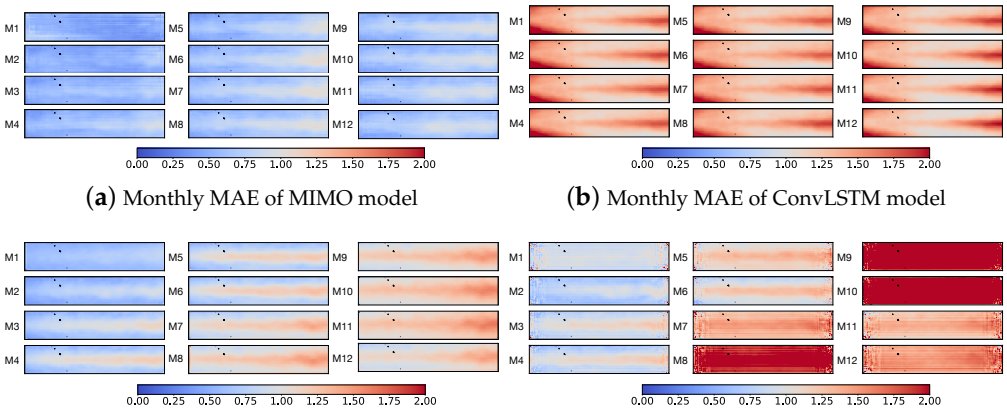

(**a**) Monthly MAE of MIMO model (**b**) Monthly MAE of ConvLSTM model

(**c**) Monthly MAE of LeNet model (**d**) Monthly MAE of CNN model

Figure 11. The results of monthly SST prediction in *Niño* 3.4 region.

5.4. Discussion

According to the experimental evaluation, the proposed MIMO model achieves good performance in predicting SSTs of different temporal scales and outperforms multiple classical forecasting methods. The underlying principles can be explained from two aspects.

On the one hand, the dynamics of SST has short-term temporal dependency, middle-term trend and long-term periodicity. For short-term temporal dependency, the SST in the next few days is usually similar to the that of past few days. For the middle-term trend, the SST may keep increasing within a few weeks. For long-term periodicity, the SST of the same month in two consecutive years is often similar. Therefore, integrating SST predictions of different temporal scales lets us have a better understanding of the dynamics of SST from an overall review and could further enhance the prediction performance.

On the other hand, the SSTs of different temporal scales are often correlated. For example, the increase of short-term SST causes the ocean to accumulate energy, which will result in the changes of long-term SST. Meanwhile, when the energy is accumulated to a certain extent, the ocean begins to release energy. Therefore, long-term SST changes will also affect short-term SST. The proposed MIMO model can fully take advantage of such correlations to improve SST prediction.

6. Conclusions

This work proposes the multi-scale SST prediction problem and develops a new model named Multi-In and Multi-Out (MIMO) to address this problem. MIMO can fuse multi-scale SST data and external data to learn comprehensive features and decode the learned features to adaptively predict daily, weekly and monthly SST. Experimental evaluation shows that MIMO can achieve much better prediction performance than existing SST prediction methods in predicting weekly and monthly SST, and comparable prediction performance with the state-of-the-art prediction method in predicting daily SST. The superiority of MIMO lies in that it can do multi-scale SST prediction in a unified model, thus improving the prediction accuracy by capturing the correlations among different scales of SST.

Author Contributions: Conceptualization: S.H., W.L.; Methodology: S.H., W.L., T.L.; validattion: S.H.; formal analyses: S.H., W.L.; data curation: S.H., T.L.; writing—original draft preparation: S.H.; writing—review and editing: W.L., T.L., S.Z.; visualization: S.H.; supervision: J.G., R.Q., Z.W. All authors have read and agreed to the published version of the manuscript.

Funding: This research was funded by National Natural Science Foundation of China under grants No. U1936205, 62172300, Shanghai Pujiang Program under grants No. 20PJ1414300, Open Reseach Program of Shanghai Key Lab of Intelligent Information Processing under grants No. IIPL201909, and China National Scientific Seafloor Observatory.

Data Availability Statement: The OISST data used in this work are available from https://www.ncei.noaa.gov/products/optimum-interpolation-sst, accessed on 27 February 2022. The NCEP/NCAR Reanalysis 1 data in this work are available at https://psl.noaa.gov/data/gridded/data.ncep.reanalysis.html, accessed on 27 February 2022.

Conflicts of Interest: The authors declare no conflict of interest.

Appendix A. Data Alignment

Due to the different data acquisition equipment and the different resolutions of various data, it is not easy to use the data. In this work, the resolution of SST data in the *Niño* 3.4 region is $0.25^\circ \times 0.25^\circ$ and the resolution of the external factors SWR and LWR are $1^\circ \times 1^\circ$, which means that the *Niño* 3.4 area can be represented by a 40×200 matrix based on SST resolution, and a 10×50 matrix based on external factor resolution.

BCI is introduced in MIMO to align external factors from low-resolution data to high-resolution data to overcome the issue, and it is an efficient 2D data interpolation method that has been validated in several fields. The target data resolution is increased using cubic

polynomial interpolation along two axes on a two-dimensional plane. Compared with other interpolation methods, the interpolated results obtained by BCI are smoother.

Take the external data SWR as an example that needs to increase the resolution to the same size of the SST data, i.e., from $1^\circ \times 1^\circ$ to $0.25^\circ \times 0.25^\circ$. Assume the input data is SW_t at time slot t, and the output data through BCI is SW'_t at time slot t. In this work, SW'_t is 4 times larger than SW_t, i.e., scale size $s = 4$. Take a grid $SW_t'^{(i,j)}$ in SW'_t as an example, where i, j represent the row and column where the grid is located in SW'_t. To calculate the output data $SW_t'^{(i,j)}$, the $SW_t'^{(i,j)}$ needs to be proportionally scaled into the input data matrix $SW_t'^{(\frac{i}{s},\frac{j}{s})}$, i.e., $(\frac{i}{s},\frac{j}{s})$ is the position of the scaled output data in the SW_t data.

As illustrated in Figure A1, a grid in SW'_t is scaled to the position $p = (\frac{i}{s},\frac{j}{s})$ in SW_t. Taking p as the original grid and assuming that the distance between adjacent grids is 1, the BCI obtains the value of 16 adjacent grids with a maximum distance of 2 from grid p to obtain the final value of p. This can be represented by Equation (A1).

$$g(x,y) = W(d_x)AW(d_y)^T \tag{A1}$$

where A is the matrix of the nearest 16 grid value represented as follows:

$$A = \begin{pmatrix} a_{-1,-1} & a_{-1,0} & a_{-1,1} & a_{-1,2} \\ a_{0,-1} & a_{0,0} & a_{0,1} & a_{0,2} \\ a_{1,-1} & a_{1,0} & a_{1,1} & a_{1,2} \\ a_{2,-1} & a_{2,0} & a_{2,1} & a_{2,2} \end{pmatrix}$$

d_x and d_y represent the distance between the p grid and nearest 4 grids on the x and y axes, respectively. the distance $d_{x_i} = [-1-\frac{i}{s}, 0-\frac{i}{s}, 1-\frac{i}{s}, 2-\frac{i}{s}]$, and $d_{y_j} = [-1-\frac{j}{s}, 0-\frac{j}{s}, 1-\frac{j}{s}, 2-\frac{j}{s}]$. $W(\cdot)$ is the Bicubic Convolutional Kernel (BCK), i.e.,

$$W(d) = \begin{cases} (a+2)|d|^3 - (a+3)|d|^2 + 1 & |d| \le 1 \\ a(|d|^3 - 5a|d|^2 + 8a|d| - 4d & 1 < |d| \le 2 \\ 0 & |d| > 2 \end{cases} \tag{A2}$$

where a is a hyperparameter. According to the experience of other related studies [36], the value of a is set to -0.5.

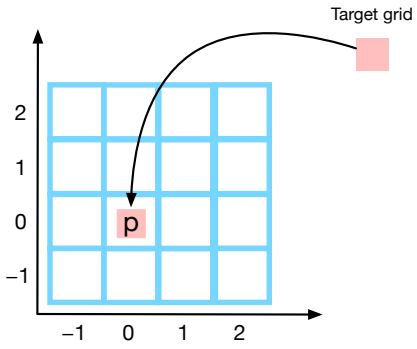

Figure A1. The bicubic mapping in BCI.

References

1. Pisano, A.; Marullo, S.; Artale, V.; Falcini, F.; Yang, C.; Leonelli, F.E.; Santoleri, R.; Buongiorno Nardelli, B. New Evidence of Mediterranean Climate Change and Variability from Sea Surface Temperature Observations. *Remote Sens.* **2020**, *12*, 132. [CrossRef]
2. Patricola, C.M.; Wehner, M.F. Anthropogenic influences on major tropical cyclone events. *Nature* **2018**, *563*, 339–346. [CrossRef] [PubMed]
3. Aemisegger, F.; Sjolte, J. A Climatology of Strong Large-Scale Ocean Evaporation Events. Part II: Relevance for the Deuterium Excess Signature of the Evaporation Flux. *J. Clim.* **2018**, *31*, 7313–7336. [CrossRef]

4. Song, Y.; Zhenning, L.; Jin-Yi, Y.; Xiaoming, H.; Wenjie, D.; Shan, H. El Niño–Southern Oscillation and its impact in the changing climate. *Natl. Sci. Rev.* **2018**, *5*, 840-857. [CrossRef]
5. Stockdale, T.N.; Balmaseda, M.A.; Vidard, A. Tropical Atlantic SST Prediction with Coupled Ocean–Atmosphere GCMs. *J. Clim.* **2006**, *19*, 6047–6061. [CrossRef]
6. Lins, I.D.; Araujo, M.; Moura, M.d.C.; Silva, M.A.; Droguett, E.L. Prediction of sea surface temperature in the tropical Atlantic by support vector machines. *Comput. Stat. Data Anal.* **2013**, *61*, 187–198. [CrossRef]
7. Wei, L.; Guan, L.; Qu, L. Prediction of Sea Surface Temperature in the South China Sea by Artificial Neural Networks. *IEEE Geosci. Remote Sens. Lett.* **2020**, *17*, 558–562. [CrossRef]
8. Garcia-Gorriz, E.; Garcia-Sanchez, J. Prediction of Sea Surface Temperatures in the Western Mediterranean Sea by Neural Networks Using Satellite Observations. *Geophys. Res. Lett.* **2007**, *34*, L11603. Available online: https://onlinelibrary.wiley.com/doi/pdf/10.1029/2007GL029888 (accessed on 17 February 2022). [CrossRef]
9. Patil, K.; Deo, M.C. Basin-Scale Prediction of Sea Surface Temperature with Artificial Neural Networks. *J. Atmos. Ocean. Technol.* **2018**, *35*, 1441–1455. [CrossRef]
10. Zhang, Q.; Wang, H.; Dong, J.; Zhong, G.; Sun, X. Prediction of Sea Surface Temperature Using Long Short-Term Memory. *IEEE Geosci. Remote Sens. Lett.* **2017**, *14*, 1745–1749. [CrossRef]
11. Zheng, G.; Li, X.; Zhang, R.H.; Liu, B. Purely satellite data–driven deep learning forecast of complicated tropical instability waves. *Sci. Adv.* **2020**, *6*, eaba1482. [CrossRef] [PubMed]
12. Xiao, C.; Chen, N.; Hu, C.; Wang, K.; Xu, Z.; Cai, Y.; Xu, L.; Chen, Z.; Gong, J. A spatiotemporal deep learning model for sea surface temperature field prediction using time-series satellite data. *Environ. Model. Softw.* **2019**, *120*, 104502. [CrossRef]
13. Carton, J.A.; Cao, X.; Giese, B.S.; Silva, A.M.D. Decadal and Interannual SST Variability in the Tropical Atlantic Ocean. *J. Phys. Oceanogr.* **1996**, *26*, 1165–1175. [CrossRef]
14. Arakawa, O.; Kitoh, A. Comparison of Local Precipitation–SST Relationship between the Observation and a Reanalysis Dataset. *Geophys. Res. Lett.* **2004**, *31*, L12206. Available online: https://onlinelibrary.wiley.com/doi/pdf/10.1029/2004GL020283 (accessed on 21 February 2022). [CrossRef]
15. Zafarparandeh, I.; Lazoglu, I. 4-Application of the finite element method in spinal implant design and manufacture. In *The Design and Manufacture of Medical Devices*; Davim, J.P., Ed.; Woodhead Publishing Reviews: Mechanical Engineering Series; Woodhead Publishing: Sawston, UK, 2012; pp. 153–183. [CrossRef]
16. Grotch, S.L.; MacCracken, M.C. The Use of General Circulation Models to Predict Regional Climatic Change. *J. Clim.* **1991**, *4*, 286–303. [CrossRef]
17. Krishnamurti, T.N.; Chakraborty, A.; Krishnamurti, R.; Dewar, W.K.; Clayson, C.A. Seasonal Prediction of Sea Surface Temperature Anomalies Using a Suite of 13 Coupled Atmosphere–Ocean Models. *J. Clim.* **2006**, *19*, 6069–6088. [CrossRef]
18. Aparna, S.G.; D'Souza, S.; Arjun, N.B. Prediction of daily sea surface temperature using artificial neural networks. *Int. J. Remote Sens.* **2018**, *39*, 4214–4231. [CrossRef]
19. Khemchandani, R.; Goyal, K.; Chandra, S. TWSVR: Regression via Twin Support Vector Machine. *Neural Netw.* **2016**, *74*, 14–21. [CrossRef]
20. Kumar, C.; Podestá, G.; Kilpatrick, K.; Minnett, P. A machine learning approach to estimating the error in satellite sea surface temperature retrievals. *Remote Sens. Environ.* **2021**, *255*, 112227. [CrossRef]
21. Lins, I.; Moura, M.; Silva, M.; Droguett, E.; Veleda, D.; Araujo, M.; Jacinto, C. Sea surface temperature prediction via support vector machines combined with particle swarm optimization. In Proceedings of the 10th International Probabilistic Safety Assessment & Management Conference, Seattle,WA, USA, 7–11 June 2010.
22. Dommenget, D.; Jansen, M. Predictions of Indian Ocean SST Indices with a Simple Statistical Model: A Null Hypothesis. *J. Clim.* **2009**, *22*, 4930–4938. [CrossRef]
23. Wu, A.; Hsieh, W.W.; Tang, B. Neural network forecasts of the tropical Pacific sea surface temperatures. *Neural Netw.* **2006**, *19*, 145–154. [CrossRef] [PubMed]
24. Chaudhari, S.; Balasubramanian, R.; Gangopadhyay, A. Upwelling Detection in AVHRR Sea Surface Temperature (SST) Images using Neural-Network Framework. In Proceedings of the IGARSS 2008—2008 IEEE International Geoscience and Remote Sensing Symposium, Boston, MA, USA, 8–11 July 2008; Volume 4, pp. IV–926–IV–929; ISSN 2153-7003. [CrossRef]
25. Wu, Z.; Jiang, C.; Conde, M.; Deng, B.; Chen, J. Hybrid improved empirical mode decomposition and BP neural network model for the prediction of sea surface temperature. *Ocean. Sci.* **2019**, *15*, 349–360. [CrossRef]
26. Patil, K.; Deo, M.C. Prediction of daily sea surface temperature using efficient neural networks. *Ocean. Dyn.* **2017**, *67*, 357–368. [CrossRef]
27. LeCun, Y.; Bengio, Y.; Hinton, G. Deep learning. *Nature* **2015**, *521*, 436–444. [CrossRef]
28. Ham, Y.G.; Kim, J.H.; Luo, J.J. Deep learning for multi-year ENSO forecasts. *Nature* **2019**, *573*, 568–572. [CrossRef]
29. Xiao, C.; Chen, N.; Hu, C.; Wang, K.; Gong, J.; Chen, Z. Short and mid-term sea surface temperature prediction using time-series satellite data and LSTM-AdaBoost combination approach. *Remote Sens. Environ.* **2019**, *233*, 111358. [CrossRef]
30. Yao, G.; Liu, Z.; Guo, X.; Wei, C.; Li, X.; Chen, Z. Prediction of Weather Radar Images via a Deep LSTM for Nowcasting. In Proceedings of the 2020 International Joint Conference on Neural Networks (IJCNN), Glasgow, UK, 19–24 July 2020; pp. 1–8; ISSN 2161-4407. [CrossRef]

31. Weyn, J.A.; Durran, D.R.; Caruana, R. Can Machines Learn to Predict Weather? Using Deep Learning to Predict Gridded 500-hPa Geopotential Height From Historical Weather Data. *J. Adv. Model. Earth Syst.* **2019**, *11*, 2680–2693. Available online: https://agupubs.onlinelibrary.wiley.com/doi/pdf/10.1029/2019MS001705 (accessed on 3 March 2022). [CrossRef]
32. Zhang, K.; Geng, X.; Yan, X.H. Prediction of 3-D Ocean Temperature by Multilayer Convolutional LSTM. *IEEE Geosci. Remote Sens. Lett.* **2020**, *17*, 1303–1307. [CrossRef]
33. Zhang, X.; Li, Y.; Frery, A.C.; Ren, P. Sea Surface Temperature Prediction With Memory Graph Convolutional Networks. *IEEE Geosci. Remote Sens. Lett.* **2021**, *19*, 1–5. [CrossRef]
34. Yu, F.; Koltun, V. Multi-Scale Context Aggregation by Dilated Convolutions. In Proceedings of the 4th International Conference on Learning Representations, ICLR 2016, San Juan, Puerto Rico, 2–4 May 2016.
35. Timothy, D. Incorporating nesterov momentum into adam. *Nat. Hazards* **2016**, *3*, 437–453.
36. Keys, R. Cubic convolution interpolation for digital image processing. *IEEE Trans. Acoust. Speech Signal Process.* **1981**, *29*, 1153–1160. [CrossRef]